Materials Advances

PAPER

Check for updates

Meniscus-confined capping-free 3D printed gold nanoparticles for quantitative SERS detection of bisphenol A†

Netrapal Singh,[ab] Manoj Kumawat,[c] Hafsa Siddiqui, [iD][b]
Koyalada Bhavani Srinivas Rao,[b] Satendra Kumar,[ab] Manoj Goswami,[ab]
Sathish Natarajan,[ab] Mohammed Akram Khan,[ab] Avanish Kumar Srivastava [iD][ab] and
Surender Kumar [iD] *[ab]

Exposure to plasticizers may lead to serious health problems in humans; hence, a rapid technique to quantitatively detect their ultra-low concentrations is highly required. The surface-enhanced Raman spectroscopy (SERS) technique has gained popularity regarding plasticizer detection. The present study demonstrated meniscus-confined electrochemically 3D printed capping agent-free gold nanoparticles (3DPAu) as a SERS substrate for quantitatively detecting one of such common plasticizers, bisphenol A (BPA). The 3DPAu substrates of 14 nm size are fabricated using a meniscus of 0.8 mm size at 0.4 mm s^{-1} printing speed and 2.5 V potential using the localized redox chemistry process. The 3DPAu substrates are fabricated without using any capping agents, which helps in enhancing their SERS activity as the capping agents increase the gap between the metal nanoparticles and analyte molecules, which in turn results in abrupt decay of the enhancement in the Raman signal. The BPA detection limit is as low as 0.25 ppm, lower than the standard value prescribed for human intake (0.6 ppm). The 3DPAu electrodes showed excellent repeatability (tested 36 times) and reproducibility (tried 5 times). The relative standard deviation (RSD) values for repeatability and reproducibility are only 4.9 and 2.6%, respectively. The ability to retain up to 89% of the initial SERS signal value, even after a long period of 7 weeks, indicated the long-term stability of the 3DPAu substrates. Furthermore, the leached-out BPA concentration from the commercial plastic products is also quantified to test the suitability of 3DPAu substrates for analyzing actual samples. This work also proposes a possible mechanism for BPA SERS detection through 3DPAu substrates.

1. Introduction

Plasticizers are one of the most common ingredients in the plastic industry, making plastic products more flexible, durable, transparent, and ductile.[1,2] BPA is one such widely used plasticizer. It is a synthetic organic compound used in various plastic industries to make epoxy resins, polycarbonate plastics, and thermal papers for different consumer goods and industrial products.[3,4] Studies found that BPA can leach out from plastic components and thus be released into the environment. The release of BPA is possible at any stage of its life cycle, *i.e.*

production, consumption, or disposal, and it can further migrate into beverages or food and possibly be ingested.[3,5] Food, water, and contaminated air are considered the primary sources of human exposure. Numerous studies have proven that it has endocrine-disrupting properties, resulting in various health hazards for the metabolic, reproductive, immune, and nervous systems, along with the formation and growth of offspring.[6,7] Thus, ultrasensitive methods for BPA detection at low levels become very important. Liquid chromatography, liquid chromatography-mass spectroscopy, gas chromatography-mass spectrometry, capillary electrophoresis, enzyme-linked immunosorbent assay, immunochromatographic assay, molecularly imprinted polymer-based sensors, aptamer-based sensors, and electrochemical sensors are commonly used BPA detection analytical methods.[8,9] However, the requirement of unique extraction processes, complex sample pretreatments, bulky instruments, a stable laboratory environment, longer reaction time, and costly antibodies restricts their use for BPA detection.[10] Hence, developing a rapid, reliable, low-cost, repeatable, and ultrasensitive

^{a} *Academy of Scientific and Innovative Research (AcSIR), Ghaziabad-201002, India.*
  E-mail: surenderjanagal@gmail.com, surender@ampri.res.in

^{b} *CSIR-Advanced Materials and Processes Research Institute (AMPRI), Bhopal-462026, India*

^{c} *CMR-National Institute for Research in Environmental Health, Bhopal-462030, India*

† Electronic supplementary information (ESI) available. See DOI: https://doi.org/10.1039/d3ma00851g

method for quantitative BPA detection is still the need of the hour. In recent years, the SERS technique has provided a rapid and label-free reliable solution for detecting BPA with appreciable detection limits.[11–13]

SERS enhances the original Raman signal obtained by the inelastic scattering of the incident radiation by an analyte molecule. This occurs when the analyte is adsorbed or connected to a noble metallic (gold, silver) surface. The enhancement in the original Raman signal can go beyond the order of 10^8, which enables the pathway for even single molecule detection.[14] There is enough evidence in the literature that it can be concluded that the origin of this process results from localized surface plasmon resonance (LSPR) in metallic nanostructures.[15] LSPs are highly localized coherent oscillations of metallic free electrons, which get resonant when their oscillation frequency matches that of the incident light. This, in turn, produces the LSPR phenomenon.[16] This resonant frequency strongly depends on factors such as the composition, shape, dimensions, dielectric atmosphere, and distance among the adjutant nanoparticles (NPs). Also, the NPs' size should be one-tenth of the wavelength of the incident light to have strong plasmon coupling and, consequently, assertive LSPR behaviour.[17] This LSPR phenomenon is responsible for the electromagnetic enhancement of the original Raman signal. The enhancement is found to be maximum in between the "hotspot" region. The hotspot regions are formed when the nanostructures are adjusted so that the gap between two adjustment nanostructures is of the order of a few nanometers.[18,19] The SERS, being the Raman process, generates the enhanced "fingerprints" of the analyte molecules.[20]

Gold-based nanostructures are among the most widely used SERS substrates among various noble metallic nanostructures because of their high tunability, biocompatibility, and unique electronic and optical properties.[21] Furthermore, gold nanostructures have a more nontoxic nature and higher stability than similar nanomaterials.[21] Various methods such as electrodeposition, de-alloying, photochemical deposition, chemical routes, plasma etching, ion sputtering, focus ion beam, lithography, laser ablation, inkjet printing, screen printing, and dip-coating, *etc.*, have been employed to obtain high-quality and reproducible gold-based SERS substrates.[18,22–26] Although most of these methods are able to get the job done, problems like controlling uniformity and reproducibility, longer reaction time, high production cost, and use of toxic chemicals are associated in one way or another with the methods above and hence new approaches to obtain high quality, uniform, and reproducible gold SERS substrates are still required. One such process to fabricate metallic SERS substrates is meniscus-confined electrochemical 3D printing (MC-E3DP).[27]

The MC-E3DP process works on the principle of a localized electrodeposition process.[28,29] In this process, the electrolyte of interest is filled in a syringe-nozzle system attached to the printhead of a 3D printer. A metal rod dipped into the electrolyte acts as an anode, while a conductive substrate serves as the working cathode electrode. When the nozzle is brought in contact with the conductive substrate, a liquid electrolyte bridge is formed between the nozzle tip and the conductive

substrate. This liquid bridge is known as the meniscus and acts as the virtual electrochemical cell between the conductive substrate and anode.[30] On applying a suitable potential, the localized electrodeposition starts through the meniscus. The movement of the meniscus is governed by the desired computer-aided design (CAD) files, which adds the flavour of AM to the process. Thus, the desired metallic structures can be obtained by controlling the meniscus in the *x*, *y*, and *z*-directions.[30,31] Furthermore, control up to atomic scale deposition can be achieved by controlling the electrodeposition parameters, *i.e.* concentration of electrolyte, applied potential and AM parameters, *i.e.* nozzle-tip size, printing speed, and meniscus height.[32]

In this work, for the first time, we are reporting MC-E3DP capping agent-free gold nanoparticles as highly reproducible (tested 5 times) SERS substrates. The printing of 3DPAu substrates is done using a nozzle of 0.8 mm tip diameter, and a meniscus of a height of 0.1 mm was maintained during the printing process. The meniscus is further allowed to move across the space (*x*, *y*, & *z*) as per the provided G-code file at 0.4 mm s^{-1} printing speed and a 2.5 V deposition potential is applied to carry out the desired localized redox deposition process. The purity of 3DPAu SERS substrates is characterized through various analysis tools, and these substrates are used for the quantitative SERS detection of BPA. The 3DPAu SERS substrates can detect as low as 0.25 ppm BPA concentration. Furthermore, repeatability (tested 36 times), stability (tested for 7 weeks), and selectivity (tested using 4 similar compounds) studies are also carried out, and appreciable results are observed. The suitability of 3DPAu substrates for analyzing real samples is also investigated using commercial plastic products.

2. Experimental section

2.1. Materials

Tetrachloroauric acid hydrate (HAuCl$_4$·3H$_2$O, ultrapure-99.99%) and acetone (ultrapure, ACS reagent-99.5%) were procured from SRL Chemicals. Indium tin oxide (ITO)-coated glass plates (sheet resistance $\sim 10 \Omega$ cm^{-2}) and platinum wire were purchased from a commercial vendor Global Nanotech Pvt. Ltd. The standard solutions of bisphenol A (BPA), phthalate esters (PAEs) mix, benzyl butyl phthalate (BBP), bis(2-ethylhexyl)phthalate (DEHP), diethyl phthalate (DEP), and dimethyl phthalate (DMP) in methanol were purchased from AccuStandard. Methanol (HPLC grade, 99.8%) was procured from S.D. Fine-Chem Ltd. Isopropyl alcohol (IPA, 99.5%) was purchased from Sigma-Aldrich. Double-distilled water was used throughout the experiments. No further purification was done for any as-received chemicals.

2.2. Instruments

The cyclic voltammetry (CV) study of 5 mM HAuCl$_4$ aqueous solution was done using a CHI-660E electrochemical instrument. The 3DPAu substrates were prepared using an in-house built meniscus-confined electrochemical 3D printer, MCube 3D ElectroDip. The purity of the 3DPAu substrates was characterized

through various tools. The crystallographic phase analysis used a Rigaku Miniflex X-ray diffractometer (XRD). The XRD was equipped with Cu-K$_\alpha$ monochromatic radiation of 1.542 Å wavelength. Field emission scanning electron microscopy (FESEM) was performed using a Thermo Fisher FEI-Quanta 250 FEG facilitated with an energy dispersive X-ray spectroscopy (EDS) detector for morphological and elemental mapping study. Transmission electron microscopy (TEM) analysis was done using a JEOL JEM F-200 TEM at 200 kV. An Evolution, 220 UV-Visible Spectrometer by Thermo Scientific, was used to obtain the UV-Vis-NIR spectra. The chemical state was analyzed using X-ray photoelectron spectroscopy (XPS), which was carried out using Thermo Fisher Scientific Instruments, U.K., having an X-ray source of Al-K$_\alpha$ (Monochromatic) with 6 mA beam current and 12 kV operating voltage. Normal and surface-enhanced Raman spectroscopic measurements were taken using an IndiRam CTR-300 Raman spectrometer with a 532 nm diode laser and operated at ~20 mW of laser power. All the Raman spectra were collected using a 50× objective lens, and the total time of the cumulative accumulations was 30 seconds.

2.3. Preparation method of 3DPAu substrates

Fig. 1 shows a schematic of the 3D printer. The system was equipped with a syringe-nozzle system attached to its print head. Here, 5 mM HAuCl$_4$ aqueous solution was filled in the syringe to be used as the precursor electrolyte, and Pt-wire dipped into this electrolyte was used as the anode material, while indium tin oxide (ITO) coated glass plates served as conductive working electrodes. The back end of the syringe was closed using a cork to maintain the required back pressure. The ITOs were cleaned using a soap solution followed by acetone, IPA, and distilled water and dried using a hair dryer before use. The requisite structures were first designed using CAD software, further sliced in a G-code file, and finally supplied to the 3D printer. A 0.8 mm tip diameter nozzle was used, and the meniscus of the height of 0.1 mm was maintained during the printing process. The meniscus height was decided based on the values provided in the earlier reported studies.[33,34] The 3DPAu preparation was carried out by moving the meniscus across the space (x, y, & z) as per the provided G-code file at 0.4 mm s^{-1} printing speed and a 2.5 V deposition potential. The cyclic voltammetry (CV) study of precursor

electrolytes was first done to determine the optimum deposition potential. The CV study was carried out using a similar two-electrode setup that was used for the preparation of the 3DPAu substrate. Fig. S1 of the ESI† shows two oxidation (labelled as O1 and O2) and two major reduction (labelled as R1 and R2) peaks. The optimum deposition potential was chosen to be 2.5 V (higher than the value corresponding to the second reduction peak R2, *i.e.* −2.3 V) because, during the MC-E3DP process, the nozzle would be in a continuous movement at a particular speed (0.4 mm s^{-1} here). Hence, some overpotential might be required for the proper deposition of 3DPAu substrates.

2.4. Sample preparation for the SERS study

Methanol solutions of different BPA concentration (1000, 100, 10, 1, 0.5, 0.25 ppm) were prepared by the series dilution method using the standard BPA solution. A 20 μL aliquot of these solutions was drop-cast onto the 3DPAu substrates to carry out the SERS measurements. Fig. 2a shows the schematic representation of the sample preparation for the SERS study. 230 000 ppm methanol solution of BPA was prepared and drop-cast similarly onto the bare ITO plate to collect the normal Raman spectra. A 10 ppm standard solution of phthalate esters (PAEs) mix, benzyl butyl phthalate (BBP), bis(2-ethylhexyl)phthalate (DEHP), diethyl phthalate (DEP), and dimethyl phthalate (DMP) in methanol were drop-cast on 3DPAu for the selectivity study. All the samples mentioned above were left to dry naturally under ambient conditions at room temperature before the SERS measurements were taken.

3. Results and discussion

3.1. Characterizations

Fig. 2b shows the X-ray diffraction (XRD) diffraction pattern spectra of 3DPAu substrates on the ITO plate. The observed spectra have major XRD peaks of gold corresponding to its face-centered cubic (FCC) crystal structure, which are well-matched with the standard JCPDS no. 04-0784.[35] Interplanar distances (*d*-spacing) are also calculated for 3DAu using the standard
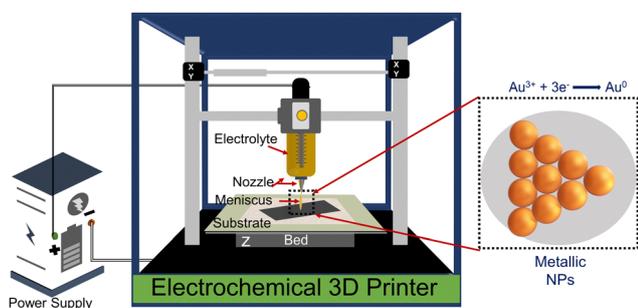

Fig. 1 Schematic representation of the MC-E3DP to prepare 3DPAu substrates.
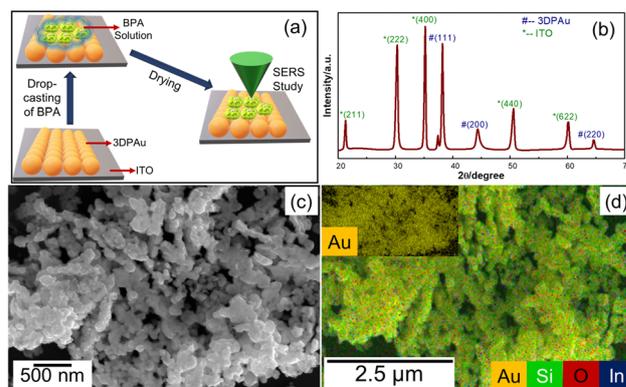

Fig. 2 (a) Schematic of SERS sample preparation, (b) XRD patterns, (c) FESEM image, and (d) EDS map of 3DP Au; the inset shows the complete EDS map corresponding to gold.

Bragg's equation for XRD. The d-spacing values are found to be 0.24, 0.20, and 0.14 nm for (111), (200), and (220) planes of gold, respectively. The average value of crystal lattice parameter (a) is calculated to be 0.41 nm. All these values agree with standard values for gold.[36] Additionally, the peaks of ITO are also found (JCPDS no. 06-0416) due to its use as the base electrode for 3DPAu.[37] No sign of other impurities is found in the XRD patterns. Thus, the XRD patterns confirmed the phase purity of 3DPAu.

The morphological characteristics of 3DPAu were initially studied using field emission scanning electron microscopy (FESEM). The low magnification micrograph (Fig. S2 of ESI†) reveals the aggregated growth of neighboring gold nanoparticles. Remarkably, the surface morphology of the 3DPAu reveals well-dispersed nanoparticles. This clearly shows that the 3D nanoparticles entirely cover the ITO electrode surface. The clusters of 3DAu are shown more clearly in Fig. 2c at higher magnification. Fig. 2d shows the energy dispersive X-ray spectroscopy (EDS) mapping of the 3DPAu substrate and confirms the formation of pure gold nanoparticles as there exist no other elements except for indium (In), silicon (Si) and oxygen (O). These elements belong to the ITO glass plate, where the Au nanoparticles were 3D printed.

TEM micrographs of Fig. 3a and b highlighted that the morphology of most of the nanoparticles of the 3DPAu substrates is elongated, circled, and shaped with a significant deviation from circularity. The morphology can be said to have an elliptical shape. The agglomeration of the gold nanoparticles in 3DPAu substrates is still observed and possibly presents the so-called "hotspots" during the SERS measurements. The inset

of Fig. 3b shows the high-resolution TEM (HR-TEM) image, which was used to calculate the d-spacing value of the 3DPAu nanoparticles. The calculated d value is 0.24 nm, which corresponds to the (111) plane of the FCC gold and matches very well with the corresponding value calculated using XRD. The average size of the nanoparticles of the 3DPAu substrates was further calculated using the TEM micrographs and came out to be 14 nm. Most particles can be found in a narrow range of 6–26 nm. The selected area electron diffraction (SAED) patterns (Fig. 3d) reveal the pure polycrystalline nature of the 3DPAu substrates and are in complete agreement with the XRD patterns of Fig. 2b.

The UV-Vis spectrum of the 3DPAu substrate was collected to study its plasmonic band, as the metals show the UV-Vis peaks corresponding to their surface plasmon resonance (SPR) wavelength. Since SERS is based on these localized SPRs, the study becomes significant in finding a suitable Raman excitation wavelength for SERS measurements. The UV-Vis spectra of 3DPAu, presented in Fig. 4a, showed two peaks, one at 380 nm and the other at 570 nm. The origin of the two peaks can be attributed to the morphology of the nanoparticles of the 3DPAu substrates. As shown earlier by SEM and TEM studies, the nanoparticles of 3DPAu substrates are elongated circles and have agglomeration; these two UV-Vis peaks would occur corresponding to transverse and longitudinal modes of the SPR of the 3DPAu nanoparticles. In this case, the peak at 380 nm corresponds to the transverse mode, and the one at 570 nm corresponds to the longitudinal mode.[38,39] Since the longitudinal SPR mode plays a crucial role in SERS measurements,[40] we have chosen a 532 nm (in range to 570 nm) laser for the SERS study in the present work.

Fig. 4b shows the X-ray photoelectron spectroscopy (XPS) data of the Au-4f state of the 3DPAu substrates. The doublet peaks at 83.7 and 87.4 eV correspond to the energy levels $4f_{7/2}$ and $4f_{5/2}$ of pure elemental gold, i.e. the Au^0 state. The observed energy separation (Δ) between the doublet peaks is 3.7 eV, consistent with the reported values in the literature.[41] The complete XPS survey is shown in Fig. S3 of the ESI.† It can be seen that only peaks of In, Sn, O, and C elements are observed other than Au. The In-3d, 3p, Sn-3d, 3p, and O-1s peaks correspond to the ITO, while the C-1s peak belongs to the adventitious carbon.[42,43] The absence of any other peak than the peaks described above indicated that the 3DPAu is made of pure elemental gold with no trace of impurities.
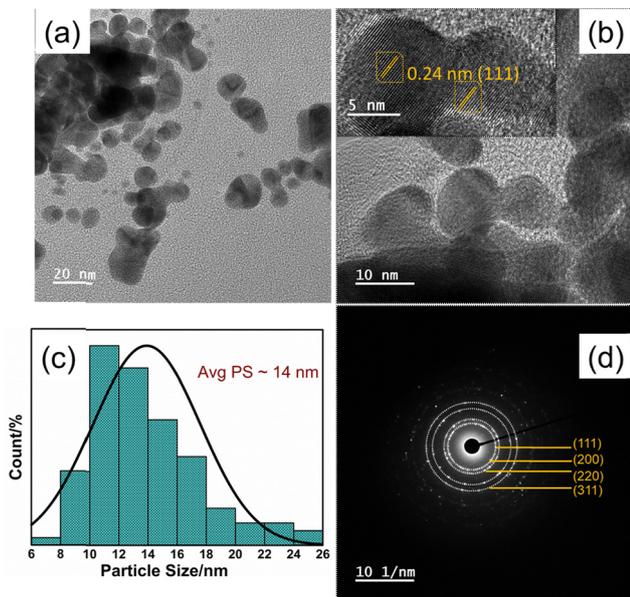

Fig. 3 (a) TEM image at low magnification, (b) TEM image at high magnification (the inset shows the corresponding HRTEM image and the d-spacing value corresponding to the (111) plane), (c) plot for particle size distribution calculated using the TEM micrograph, and (d) SEAD patterns with corresponding (hkl) values of 3DP Au.
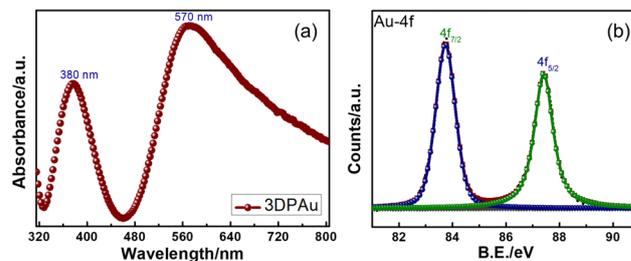

Fig. 4 (a) UV-Vis spectra and (b) high-resolution XPS spectra of Au-4f for 3DPAu.

3.2. SERS study for BPA detection

Fig. 5a shows the Raman spectra of bare ITO, the 3DPAu substrate, and 10^3 ppm BPA drop-cast on the 3DPAu substrate (10^3 ppm BPA@3DPAu). The bare ITO shows no Raman peak except for one broader peak at 1090 cm^{-1}. The observed peak is consistent with the literature.[44] The 3DPAu substrate showed no peaks, indicating the typical Raman behaviour of a metallic surface. All six major characteristic peaks are identified in the spectra of 1000 ppm BPA@3DPAu and indexed as 1, 2, 3, 4, 5, and 6. The peaks 1 and 2 at 1116 and 1183 cm^{-1} contribute to the in-plane C–H wagging vibration mode.[12] The peaks 3 (1235 cm^{-1}) and 4 (1264 cm^{-1}) belong to C–O stretching vibration.[3] The peaks 5 (1616 cm^{-1}) and 6 (3067 cm^{-1}) are associated with the phenyl ring stretching and phenyl-hydrogen stretching.[3,45] Fig. 5a indicates that the base ITO and 3DPAu substrate do not interfere with BPA detection.

The comparative study of the normal Raman and SERS spectra of BPA is shown in Fig. 5b. As can be seen, the SERS of BPA spectra is significantly enhanced compared to the corresponding normal Raman spectra though the SERS measurements are done on lower concentrations. The analytical enhancement factors (AEFs) for each characteristic BPA peak are calculated using the following equation:

$$AEF = (I_{SERS}/I_{NR}) \times (C_{NR}/C_{SERS}), \qquad (1)$$

where I_{SERS} and I_{NR} are the integrated intensities observed from SERS and normal Raman spectra. While C_{SERS} and C_{NR} stand for concentrations used during SERS and normal Raman measurements, respectively.[46,47] The detailed calculations are provided in detail in Section S1 of the ESI.† The average AEF comes out to be ∼10^4, which is quite a significant enhancement compared to the original Raman signal.

For quantitative detection of BPA on the 3DPAu substrates, SERS signals for various concentrations of BPA, ranging from 1000 to 0.25 ppm, were recorded and are shown in Fig. 5c. A strong SERS signal at 1000 ppm BPA was observed, which goes on diluting concerning lowering the BPA concentration. The SERS is detectable up to 0.25 ppm, which is considered the lower limit of the 3DPAu SERS substrates. This value is lower than the standard limit (0.6 ppm) set by the European Union migration for BPA in food intake.[48,49] These data were further analyzed by studying the relationship between the SERS peak intensities and BPA concentrations. For this purpose, we selected the characteristic BPA peak at 1616 cm^{-1} as the reference and then plotted the SERS peak intensity *versus* the BPA concentration curve on a logarithmic scale. Fig. 5d exhibits a linear relationship between SERS peak intensity (I) logarithmic values and BPA concentration (C). The corresponding linear regression equation comes out as $\log(I) = 0.18\log(C) + 3.98$, with a correlation coefficient (R^2) of 0.997. This equation will allow quantitative detection of unknown BPA concentrations in actual samples. Furthermore, the LOD is also calculated using the equation:

$$LOD = 3.3 \times \left(\frac{\text{standard deviation of the blank}}{\text{slope of the calibration curve}}\right), \qquad (2)$$

which also comes out as ∼0.25 ppm, *i.e.* the value suggested earlier.

3.3. Enhancement mechanism of the 3DPAu SERS substrate

There are two popular and well-accepted mechanisms for significant enhancement of the original Raman signal in the SERS phenomenon: (1) electromagnetic enhancement mechanism (E.M.) and (2) chemical enhancement mechanism (CM). In EM, the LSPR increases the local electric field near the NPs and provides a larger Raman cross-section to the analyte molecule, which results in a significant signal enhancement. Here, the enhancement value varies in proportion to the fourth power of the local electric field. However, in the case of CM, the charge transfer between the analyte molecules and metal NPs forms an adsorbate-surface complex. This results in a polarizability change, which again provides a larger Raman cross-section and, consequently, an enhanced signal (up to 10^2). The difference in polarizability also leads to shifts in the SERS peaks compared to the original Raman peaks. As shown in Fig. 5, there are no appreciable peak shifts (within the limit of the instrument) in the SERS of BPA through 3DPAu substrates, and a significant signal enhancement (∼10^4) is observed; it can safely be concluded that a significant portion of the signal enhancement here comes from the E.M. Scheme 1 shows the schematic representation of the enhancement of the BPA Raman signal *via* the 3DPAu substrate. Fig. 5 and AEF calculations also show that all the peaks are not enhanced equally. This can be explained based on the so-called "surface selection rules" applied in SERS, which states that the analyte molecules adsorb on the metal NP surface in some specific orientation concerning the normal of the surface. This orientation is different from that of the direct analyte molecule. Since the
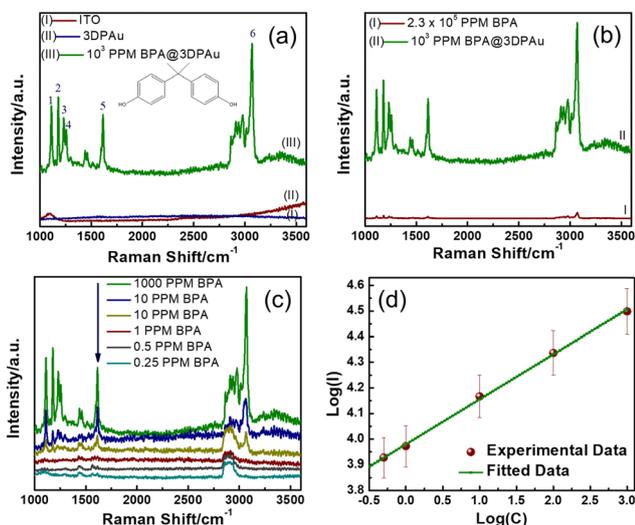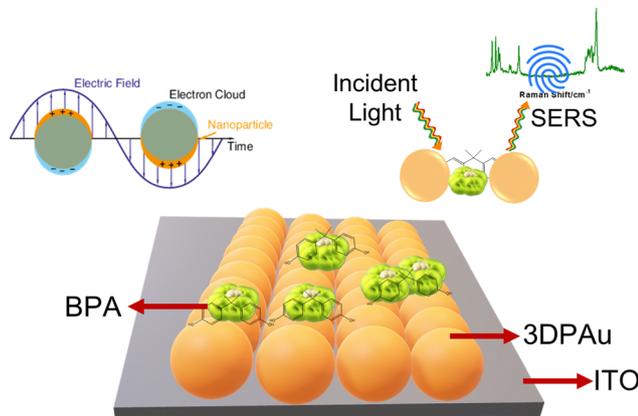

Fig. 5 (a) Raman spectra of bare ITO, 3DPAu, and BPA@3DPAu (the numbers correspond to the various peaks of BPA, and the inset shows its chemical structure), (b) normal Raman and corresponding SERS of BPA, (c) SERS of BPA at different concentrations, and (d) calibration curve corresponding to the log values of peak intensity and concentrations for the BPA peak at 1616 cm^{-1}.

Scheme 1 Schematic representation of the Raman signal mechanism of the 3DPAu substrate.

molecules' orientation plays a vital role in deciding the intensity of a particular Raman mode and hence the SERS mode, some of the modes will have more SERS intensity than others. Here, the SERS mode corresponding to the peaks 4 and 5 of the BPA Raman signal indicates their most suitable orientation compared to the other respective modes.

Moreover, the uniform hotspot regions (shown in Fig. 2 and 3) would help in the repeatability and reproducibility of the SERS signal. The following section (Section 3.4) provides the repeatability and reproducibility studies. These studies showed that deficient (<5%) RSD values indicate the uniformity of the SERS substrates prepared by the MC-E3DP process.

3.4. Repeatability, reproducibility, and stability study of the 3DPAu SERS substrate

A repeatability study shows the quality of the SERS substrates by comparing uniformity in signals of SERS spectra collected at various random spots. SERS spectra of 100 ppm BPA@3DPAu at 36 random locations were collected and compared. Fig. S4a of

Fig. 6 (a) Repeatability plot, (b) reproducibility plot, (c) stability plot, and (d) selectivity study of the 3DPAu SERS substrates. All relative intensity values correspond to the BPA peak at 1616 cm^{-1}.

the ESI† shows the corresponding spectra. The relative intensities corresponding to the characteristic peak at 1616 cm^{-1} are provided in Fig. 6a. It shows that the RSD values are only 4.9%, which indicates that the 3DPAu substrates exhibit excellent repeatability.

The reproducibility study was carried out to visualize the capability of the MC-E3DP process to reproduce similar 3DPAu substrates. A set of 5 different 3DPAu substrates was prepared, and the SERS spectra for 100 ppm BPA detection were recorded (Fig. S4b of ESI†). The 1616 cm^{-1} characteristic peak's relative intensity values are plotted and shown in Fig. 6b. A meagre RSD value (only 2.6%) points towards the high reproducibility of the MC-E3DP process for preparing the 3DPAu SERS substrates.

The long-term stability of the 3DPAu substrates was also investigated. For this study, 3DPAu substrates were stored at ambient conditions at room temperature with no special storage conditions applied. The SERS spectra were recorded weekly for a BPA concentration of 100 ppm. Fig. 6c shows the relative peak intensities corresponding to the 1616 cm^{-1} BPA characteristic peak. All the peak intensity values are the average intensity values of 3 different SERS spectra of the various substrates. The 3DPAu substrates exhibited approximately 89% intensity of the corresponding initial SERS intensity. This shows that our 3DPAu substrates possess good long-term stability and can be used without loss of any SERS signal for up to 7 weeks. A comparison of the 3DPAu substrates with various Au-based substrates is provided in Table 1.

As it can be seen from Table 1, the 3DPAu substrates showed an excellent limit of detection in comparison with the traditionally fabricated Au-based substrates, which indicated the practical feasibility of the 3DPAu substrates. This can be attributed to the fact that no capping agents are used throughout the MC-3DP process to fabricate 3DPAu substrates. These capping agents remain with the metal NPs to some extent even if multiple and meticulous washings have been employed, creating a dielectric layer around the NPs[55] The dielectric layer increases the distance between the analyte molecule and the metal NP. The theoretical and experimental observations have shown that the plasmonic field and, consequently, the SERS effect decays as D^{-12}, where D is the distance between the analyte molecule and metal NP.[56] Furthermore, the excellent repeatability and reproducibility values of the 3DPAu substrates indicate the novel features of the MC-3DP process used here, which are very hard to obtain if not impossible, as shown in Table 1.

3.5. Selectivity study of the 3DPAu SERS substrate

A good selective nature of the SERS substrates towards a target analyte indicates its practical feasibility. The selectivity of the 3DPAu SERS substrate was evaluated by measuring its response to various plasticizers that have a common presence in plastic products. The selectivity study of the 3DPAu SERS substrates is carried out using plasticizers such as BBP, DEHP, DEP, and DMP. A 10 ppm concentration of each plasticizer was independently drop-cast onto the 3DPAu substrate, and corresponding SERS measurements were done. The response of the 3DPAu
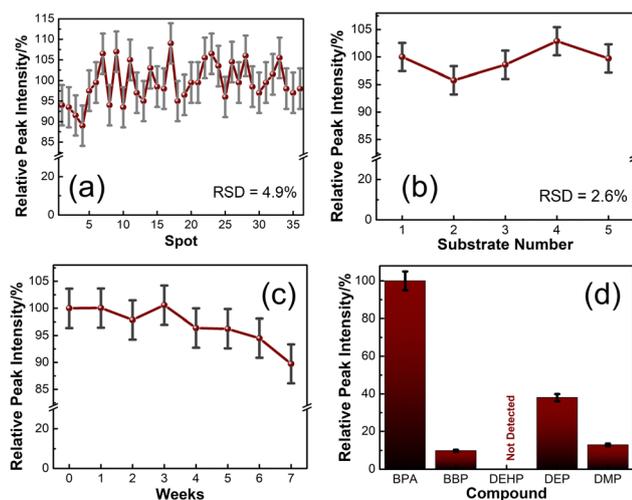
Table 1 Comparison of various gold-based SERS substrates regarding their fabrication method and LOD

SERS substrate	Method of fabrication	Analyte	LOD (ppm)	Reproducibility (RSD%)	Repeatability (RSD%)	Ref.
Au nanoparticles arrays	Liquid–liquid interfacial -assembly	Butyl benzyl phthalate	1	9.6	10.6	2
AuNR@MIP/P.S. colloid	Molecular imprinting	BPA	0.1	Not tested	8.7	12
Rough gold nanoarrays	Electrodeposition	3,3′,4,4′-Tetrachlorobiphenyl	3.4	11	6.6	50
Au NPs	Citrate reduction	Polystyrene (P.S.)	1	6.7	Not tested	51
Au NPs on flexible paper	Hydrothermal	Polyethylene terephthalate (PET)	100	7.8	5.6	52
AuNPs	Chemical route	P.S., PET	10	Not tested	Not tested	53
Au sputtered on a glass slide	Sputtering	PS	0.32	Not tested	Not tested	54
3DPAu	MC-E3DP	BPA	0.25	2.6	4.9	This work

substrates towards these compounds is shown in Fig. 6d. Here, the relative peak intensity values are plotted at the 1616 cm^{-1} peak for BPA and the maximum intensity peak value for other compounds. The 3DPAu exhibits a much lower SERS response towards other plasticizers, demonstrating the excellent selective nature of 3DPAu substrates toward BPA detection.

Furthermore, SERS spectra of a mixture of BPA and PAEs mix, each of 10 ppm, are also recorded to visualize the selective nature of 3DPAu in the presence of an interfering compound. Fig. S4c of the ESI† shows the corresponding spectra. It can be inferred that though the presence of the PAEs mix has increased the noise level of the SERS spectra, all the BPA peaks are detectable. This study further enhanced the selectivity results of the 3DPAu substrates and indicates that it has highly selective behavior towards BPA compared to other similar plasticizer compounds.

3.6. Real sample analysis for quantitative detection of BPA

To evaluate the practical feasibility of 3DPAu substrates, leached-out "real-world" samples were tested. For this purpose, commercially available drinking mineral water packaged in plastic bottles (BPA_RS-DW) and water samples (BPA_RS-BW) obtained by boiling polycarbonate baby milk bottles at 80 °C for 30 minutes were used. The BPA_RS-BW samples were cooled to room temperature under an ambient environment before testing. A set of 3 spiked concentrations of BPA (0, 100, and 200 ppm) in BPA_RS-DW and BPA_RS-BW were used for the SERS study. A 20 μL aliquot of these samples was drop-cast on 3DPAu, and after drying, SERS measurements were recorded. The corresponding SERS spectra are shown in Fig. S5 of the ESI.† It can be seen that there are no SERS spectra for the 0 ppm BPA spiked samples in both cases, which indicates that the as-obtained BPA_RS-DW and BPA_RS-BW samples either have no or below detectable BPA concentrations within the limit of our 3DPAu substrates. Recovery values are calculated using the

calibration plot of Fig. 5c for the BPA peak at 1616 cm^{-1}. Table 2 shows the recovery and RSD% values for BPA_RS-DW and BPA_RS-BW samples. The 3 sets of measurements ($n = 3$) were done for every sample. All the mean recovery values are found to be very close to the 100% values with low RSD values, which shows that our 3DPAu SERS substrates are also suitable for the quantitative detection of BPA concentrations in real samples.

4. Conclusions

In summary, the present study demonstrated the preparation method of 3DPAu substrates on ITO plates using the MC-E3DP process. The process provided a one-step solution for the fabrication of capping agent-free SERS substrates. XRD, EDS, UV-Vis, and XPS studies confirmed the purity of the 3DPAu substrates, while the FESEM and TEM images highlighted its elliptical-shaped morphology with the particles having an average size of 14 nm. The phase pure 3DPAu substrates are further used for the rapid, label-free, and quantitative SERS detection of BPA plasticizers. A wide linear range from 1000 ppm to 0.25 ppm is obtained with a lower detection limit of 0.25 ppm. The 3DPAu substrates showed an excellent limit of detection in comparison with the traditionally fabricated Au-based substrates, which indicated the practical feasibility of the 3DPAu substrates. This can be attributed to the fact that no capping agents are used throughout the MC-3DP process to fabricate 3DPAu substrates, as the capping agents tend to reduce the overall SERS signal and create interference in the measurements. The 3DPAu substrates showed remarkable reproducibility, repeatability, long-term stability, and selectivity toward BPA detection.

Furthermore, the potential of the 3DPAu substrates for real sample analysis was also tested using D. W. and B. W. samples. The 3DPAu substrates exhibited excellent recovery values in

Table 2 Real sample analysis results of BPA detection ($n = 3$)

BPA added (ppm)	BPA_RS-DW			BPA_RS-BW		
	BPA found (ppm)	Mean recovery (%)	RSD (%)	BPA found (ppm)	Mean recovery (%)	RSD (%)
0	—	—	—	—	—	—
100	99.2 ± 4.5	99.2	4.5	99.8 ± 3.8	99.8	3.8
200	201.1 ± 10.9	100.5	5.4	202.2 ± 2.9	101.1	1.4

each study, almost 100%. The proposed method offers exceptional control, making it highly suitable for creating SERS substrates tailored to specific requirements. This level of control opens up many applications in diverse fields, including medical research, industrial applications, and quality monitoring of consumer products.

Authors' contribution

Netrapal Singh: methodology, experimentation, software, data curation, writing – original draft, Manoj Kumawat: resources, review – editing, Hafsa Siddiqui: data curation, writing – editing, Koyalada Bhavani Srinivas Rao: editing and review, Satendra Kumar: validation, formal analysis, Manoj Goswami: writing – review, Sathish Natarajan: supervision, resources, Mohammed Akram Khan: supervision, review, Avanish Kumar Srivastava: resources, and Surender Kumar: conceptualization, resources, writing – review & editing.

Conflicts of interest

The authors share no conflict of interest, personal or financial.

Acknowledgements

References

1 H. Xu, J. Zhu, X. Wu, Y. Cheng, D. Wang and D. Cai, *Spectrochim. Acta, Part A*, 2023, **284**, 121735.

2 J. Liu, J. Li, F. Li, Y. Zhou, X. Hu, T. Xu and W. Xu, *Anal. Bioanal. Chem.*, 2018, **410**, 5277–5285.

3 P.-Y. Lin, C.-W. Hsieh and S. Hsieh, *Sci. Rep.*, 2017, **7**, 1–6.

4 R. Bousoumah, V. Leso, I. Iavicoli, P. Huuskonen, S. Viegas, S. P. Porras, T. Santonen, N. Frery, A. Robert and S. Ndaw, *Sci. Total Environ.*, 2021, **783**, 146905.

5 I. Cimmino, F. Fiory, G. Perruolo, C. Miele, F. Beguinot, P. Formisano and F. Oriente, *Int. J. Mol. Sci.*, 2020, **21**, 5761.

6 Y. Ma, H. Liu, J. Wu, L. Yuan, Y. Wang, X. Du, R. Wang, P. W. Marwa, P. Petlulu, X. Chen and H. Zhang, *Environ. Res.*, 2019, **176**, 108575.

7 A. Tarafdar, R. Sirohi, P. A. Balakumaran, R. Reshmy, A. Madhavan, R. Sindhu, P. Binod, Y. Kumar, D. Kumar and S. J. Sim, *J. Hazard. Mater.*, 2022, **423**, 127097.

8 A. U. Alam and M. J. Deen, *Anal. Chem.*, 2020, **92**, 5532–5539.

9 F. Sun, L. Kang, X. Xiang, H. Li, X. Luo, R. Luo, C. Lu and X. Peng, *Anal. Bioanal. Chem.*, 2016, **408**, 6913–6927.

10 D. Tu, J. T. Garza and G. L. Coté, *RSC Adv.*, 2019, **9**, 2618–2625.

11 H. L. Marks, M. V. Pishko, G. W. Jackson and G. L. Coté, *Anal. Chem.*, 2014, **86**, 11614–11619.

12 M. T. T. Nguyen, H. V. Giap, S. N. Nguyen, H. L. Nguyen, A. H. T. Vu, H. N. Nguyen and D. T. Nguyen, *Thin Solid Films*, 2022, **759**, 139465.

13 O. Guselnikova, P. Postnikov, A. Trelin, V. Švorčík and O. Lyutakov, *ACS Sens.*, 2019, **4**, 1032–1039.

14 J. Langer, D. J. de Aberasturi, J. Aizpurua, R. A. Alvarez-Puebla, B. Auguié, J. J. Baumberg, G. C. Bazan, S. E. J. Bell, A. Boisen, A. G. Brolo, J. Choo, D. Cialla-May, V. Deckert, L. Fabris, K. Faulds, F. Javier García de Abajo, R. Goodacre, D. Graham, A. J. Haes, C. L. Haynes, C. Huck, T. Itoh, M. Käll, J. Kneipp, N. A. Kotov, H. Kuang, E. C. Le Ru, H. K. Lee, J. F. Li, X. Y. Ling, S. A. Maier, T. Mayerhöfer, M. Moskovits, K. Murakoshi, J. M. Nam, S. Nie, Y. Ozaki, I. Pastoriza-Santos, J. Perez-Juste, J. Popp, A. Pucci, S. Reich, B. Ren, G. C. Schatz, T. Shegai, S. Schlücker, L. L. Tay, K. George Thomas, Z. Q. Tian, R. P. van Duyne, T. Vo-Dinh, Y. Wang, K. A. Willets, C. Xu, H. Xu, Y. Xu, Y. S. Yamamoto, B. Zhao and L. M. Liz-Marzán, *ACS Nano*, 2020, **14**, 28–117.

15 M. Moskovits, *Phys. Chem. Chem. Phys.*, 2013, **15**, 5301–5311.

16 C. Zong, M. Xu, L. J. Xu, T. Wei, X. Ma, X. S. Zheng, R. Hu and B. Ren, *Chem. Rev.*, 2018, **118**, 4946–4980.

17 E. Petryayeva and U. J. Krull, *Anal. Chim. Acta*, 2011, **706**, 8–24.

18 Z. Zuo, K. Zhu, L. Ning, G. Cui, J. Qu, Y. Cheng, J. Wang, Y. Shi, D. Xu and Y. Xin, *Appl. Surf. Sci.*, 2015, **325**, 45–51.

19 M. Fan, G. F. S. Andrade and A. G. Brolo, *Anal. Chim. Acta*, 2011, **693**, 7–25.

20 X. Luo, Y. Xing, D. D. Galvan, E. Zheng, P. Wu, C. Cai and Q. Yu, *ACS Sens.*, 2019, **4**, 1534–1542.

21 G. M. Das, S. Managò, M. Mangini and A. C. De Luca, *Nanomaterials*, 2021, **11**, 2679.

22 Q. Wang, J. Wang, M. Li, Z. Ge, X. Zhang, L. Luan, P. Li and W. Xu, *Spectrochim. Acta, Part A*, 2021, **248**, 119131.

23 E. Ashok Kumar, T. J. Wang and Y. H. Chang, *Appl. Surf. Sci.*, 2022, **585**, 152696.

24 Y. Xue, F. Scaglione, F. Celegato, P. Denis, H. J. Fecht, P. Rizzi and L. Battezzati, *Chem. Phys. Lett.*, 2018, **709**, 46–51.

25 C. Zhu, Q. Zhao, D. Huo, X. Hu and X. Wang, *Mater. Chem. Phys.*, 2021, **263**, 124388.

26 Á. I. López-Lorente, *Anal. Chim. Acta*, 2021, **1168**, 338474.

27 N. Singh, H. Siddiqui, S. Kumar, M. Goswami, A. Kumar, T. Sharda, S. Kumar, N. Sathish and A. K. Srivastava, *Mater. Lett.*, 2022, **307**, 130976.

28 X. Chen, X. Liu, P. Childs, N. Brandon, B. Wu, X. Chen, X. Liu, P. Childs, B. Wu and N. Brandon, *Adv. Mater. Technol.*, 2017, **2**, 1700148.

29 S. Morsali, S. Daryadel, Z. Zhou, A. Behroozfar, D. Qian and M. Minary-Jolandan, *J. Appl. Phys.*, 2017, **121**, 024903.

30 J. Hu and M. F. Yu, *Science*, 2010, **329**, 313–316.

31 Y. Wang, X. Xiong, B. F. Ju and Y. L. Chen, *Rev. Sci. Instrum.*, 2022, **93**, 025102.

32 J. Hengsteler, B. Mandal, C. Van Nisselroy, G. P. S. Lau, T. Schlotter, T. Zambelli and D. Momotenko, *Nano Lett.*, 2021, **21**, 9093–9101.

33 S. Morsali, S. Daryadel, Z. Zhou, A. Behroozfar, M. Baniasadi, S. Moreno, D. Qian and M. Minary-Jolandan, *J. Appl. Phys.*, 2017, **121**, 214305.

34 N. Singh, H. Siddiqui, M. Goswami, S. Kumar, M. Ashiq, N. Sathish, M. S. Santosh and S. Kumar, *ACS Appl. Nano Mater.*, 2023, **6**, 3303–3311.

35 Y. R. Lin, Y. C. Chang, Y. C. Chiao and F. H. Ko, *Catalyts*, 2022, **13**, 33.

36 V. Jeevanantham, D. Tamilselvi, S. R. Bavaji and S. Mohan, *Bull. Mater. Sci.*, 2023, **46**, 1–11.

37 Y. L. Chu, S. J. Young, H. C. Chang, S. Arya, Y. H. Liu and T. Te Chu, *ACS Appl. Electron. Mater.*, 2022, **5**, 1277–1285.

38 T. D. Tran, L. T. Le, D. H. Nguyen, M. T. Pham, D. Q. Truong, H. V. Pham, M. T. T. Nguyen and P. D. Tran, *Nanotechnology*, 2020, **31**, 265602.

39 M. Nguyen, I. Kherbouche, S. Gam-Derouich, I. Ragheb, S. Lau-Truong, A. Lamouri, G. Lévi, J. Aubard, P. Decorse, N. Félidj and C. Mangeney, *Chem. Commun.*, 2017, **53**, 11364–11367.

40 B. Peng, G. Li, D. Li, S. Dodson, Q. Zhang, J. Zhang, Y. H. Lee, H. V. Demir, X. Yi Ling and Q. Xiong, *ACS Nano*, 2013, **7**, 5993–6000.

41 B. Ananthoju, R. K. Biroju, W. Theis, R. A. W. Dryfe, B. Ananthoju, R. A. W. Dryfe, R. K. Biroju and W. Theis, *Small*, 2019, **15**, 1901555.

42 M. T. Dang, J. Lefebvre and J. D. Wuest, *ACS Sustainable Chem. Eng.*, 2015, **3**, 3373–3381.

43 J. S. Jeon, I. K. Yu, W. Kim and S. H. Choi, *Front. Chem.*, 2020, **8**, 595616.

44 M. Marikkannan, M. Subramanian, J. Mayandi, M. Tanemura, V. Vishnukanthan and J. M. Pearce, *AIP Adv.*, 2015, **5**, 017128.

45 Y. Xie, L. Ma, S. Ling, H. Ouyang, A. Liang and Z. Jiang, *Nanomaterials*, 2022, **12**, 1374.

46 Y. Liu, S. Xu, H. Li, X. Jian and W. Xu, *Chem. Commun.*, 2011, **47**, 3784–3786.

47 E. C. le Ru, E. Blackie, M. Meyer and P. G. Etchegoint, *J. Phys. Chem. C*, 2007, **111**, 13794–13803.

48 S. Almeida, A. Raposo, M. Almeida-González and C. Carrascosa, *Compr. Rev. Food Sci. Food Saf.*, 2018, **17**, 1503–1517.

49 R. Braunrath, D. Podlipna, S. Padlesak and M. Cichna-Markl, *J. Agric. Food Chem.*, 2005, **53**, 8911–8917.

50 C. Zhu, Q. Zhao, D. Huo, X. Hu and X. Wang, *Mater. Chem. Phys.*, 2021, **263**, 124388.

51 R. Yin, H. Ge, H. Chen, J. Du, Z. Sun, H. Tan and S. Wang, *Environ. Adv.*, 2021, **5**, 100096.

52 D. Xu, W. Su, H. Lu, Y. Luo, T. Yi, J. Wu, H. Wu, C. Yin and B. Chen, *Phys. Chem. Chem. Phys.*, 2022, **24**, 12036–12042.

53 J. Caldwell, P. Taladriz-blanco, B. Rothen-rutishauser and A. Petri-fink, *Nanomaterials*, 2021, **11**, 1149.

54 B. Chaisrikhwun, S. Ekgasit and P. Pienpinijtham, *J. Hazard. Mater.*, 2023, **442**, 130046.

55 M. Deb, R. Hunter, M. Taha, H. Abdelbary and H. Anis, *Spectrochim. Acta, Part A*, 2022, **280**, 121533.

56 G. Kumari, J. Kandula and C. Narayana, *J. Phys. Chem. C*, 2015, **119**, 20057–20064.